Chemical Engineering Science 291 (2024) 119924

Contents lists available at ScienceDirect

Chemical Engineering Science

journal homepage: www.elsevier.com/locate/ces

Modeling of tubular membrane contactors for ozonation of water reveals reduced bromate formation with static mixers

Stefan Herrmann [a], Maria C. Padligur [a], Conrad J. Bieneck [a], Matthias Wessling [a,b,*]

[a] RWTH Aachen University, AVT.CVT - Chair of Chemical Process Engineering, Forckenbeckstraße 51, 52074 Aachen, Germany
[b] DWI - Leibniz Institute for Interactive Materials, Forckenbeckstraße 50, 52074 Aachen, Germany

ARTICLE INFO

Keywords:
Advanced oxidation
Ozonation
Bromate formation
Membrane contactor
Simulation

ABSTRACT

Bromate formation and insufficient micropollutant degradation are two major problems in wastewater ozonation. The conventional process using bubble columns has the drawback of an inhomogeneous ozone distribution, causing increased bromate formation. Membrane contactors are a promising alternative as they can dissolve ozone bubble-free. This work presents a simulation of a tubular membrane contactor in COMSOL Multiphysics that includes flow, mass transfer, ozone decay, and reactions of organic molecules and bromide with ozone and hydroxyl radicals. Gaseous ozone and water flow on the lumen and shell side of the membrane, respectively. Static mixers are placed in the water channel, coaxial between the membrane and housing. The simulations show a 75% increase in ozone flux through the membrane, a homogenized ozone distribution, and 13 times higher degradation of a medium-oxidizable micropollutant in the presence of additional static mixers. Furthermore, static mixers enable the use of a lower gaseous ozone concentration, resulting in 31% lower bromate formation at the same ozone exposure without affecting micropollutant degradation. Overall, we demonstrate that membrane contactors with static mixers can be used as a strategy to reduce bromate formation.

1. Introduction

Ozonation is a viable process to degrade micropollutants (MP) in wastewater (Kanakaraju et al., 2018). With an ongoing increase of micropollutants that are emitted into the environment all around the world, such degradation methods become more important to protect the environment (Luo et al., 2014; Jiang et al., 2013; Kumar et al., 2020). The main points of micropollutant discharge are wastewater treatment plants (WWTPs) (Kanakaraju et al., 2018; Jiang et al., 2013). Thus, more WWTPs need to be equipped with advanced oxidation technologies, e.g. ozonation, in the future. However, ozonation as it is currently used has two major drawbacks: firstly, low degradation of some micropollutants due to insufficient ozone doses (El-taliawy et al., 2017; Zhou et al., 2015; Wardenier et al., 2019; Altmann et al., 2014), secondly, the formation of potentially harmful oxidation by-products (Sohn et al., 2004; Schollée et al., 2018) and carcinogenic bromate (Hübner et al., 2016; Krasner et al., 1993; Song et al., 1996) causing limitations of the ozone dose.

Conventional ozonation processes in wastewater treatment work with bubble columns or venturi jets (Bein et al., 2020). In venturi jet systems, a side stream is contacted with gaseous ozone in a venturi injector and subsequently mixed with the main wastewater stream. The mixing step is often promoted by static mixers (Rakness et al., 2018). In bubble columns, small ozone bubbles are introduced at the bottom of a reactor and the ozone dissolves into the water while the bubbles rise to the surface. The disadvantages of this method are foaming, large reactor footprints, loss of undissolved ozone in the reactor headspace, and unstable flow conditions with limitations in mass transfer (Bein et al., 2020; Schmitt et al., 2022; Sabelfeld and Geißen, 2019). The phase boundary between gaseous ozone and wastewater is not stable and changes throughout the reactor. Bubble coalescence is a major factor in reducing the phase boundary, which hinders ozone mass transfer (Sabelfeld and Geißen, 2019). Furthermore, unstable flow conditions result in an inhomogeneous concentration of dissolved ozone in the reactor. According to film theory, the dissolved ozone concentration is high around ozone bubbles and decreases toward the bulk phase. This concentration profile further limits the ozone mass transfer into wastewater (Smith and El-Din, 2002; Zhou et al., 1994).

The limited ozone mass transfer in bubble columns directly leads to limitations in micropollutant abatement. The three main parameters for the degradation of the micropollutant are the concentration

* Corresponding author at: RWTH Aachen University, AVT.CVT - Chair of Chemical Process Engineering, Forckenbeckstraße 51, 52074 Aachen, Germany.
E-mail address: Manuscripts.CVT@avt.rwth-aachen.de (M. Wessling).

https://doi.org/10.1016/j.ces.2024.119924
Received 12 December 2023; Received in revised form 14 February 2024; Accepted 22 February 2024
Available online 28 February 2024

Nomenclature

Abbreviations

MP	Micropollutant
WWTP	Wastewater treatment plant
UV	Ultraviolet
BOM	Background organic matter
CFD	Computational fluid dynamics
HSB	Hoigné-Staehelin-Bader
TFG	Tomiyasu-Fukutomi-Gordon
PE	Periodic element
HPC	High performance computing
PTFE	Polytetrafluoroethylene

Symbols

ρ_i	Density of component i
$\mathbf{v}$	Velocity vector
p	Pressure
μ	Dynamic viscosity
c_i	Concentration of component i
t	Time
D_i	Diffusion coefficient of component i
R_i	Reaction rate of component i
k_i	Reaction rate constant of component i
R_{ct}	Ratio of hydroxyl radicals to Ozone
$H^{cc}_{S,i}$	Henry coefficient of component i
K_L	Mass transfer coefficient
Re	Reynolds number

of ozone, the reaction kinetic of the respective micropollutant with ozone and other oxidizing species, e.g., hydroxyl radicals, generated by ozone decay, and the water matrix (Lee et al., 2013; Nawrocki et al., 2003). While micropollutants with high reaction kinetics can be easily degraded, those with slow kinetics need high contact times and high ozone concentrations to be degraded to a sufficient amount (Wünsch et al., 2022; Lee et al., 2013). To characterize the coupled effect of ozone concentration and contact time, the ozone exposure is used. Furthermore, the ozone decay to hydroxyl radicals needs to be taken into account for MP degradation. The ozone decay can be influenced by pH, water matrix, additives such as hydrogen peroxide, metal catalysts, and UV radiation (Gardoni et al., 2012; Katsoyiannis et al., 2011; Andreozzi et al., 1992). Hydroxyl radicals can react in an unselective manner with MPs; therefore, they are favorable in high concentration within the process (von Sonntag, 2007; von Sonntag and von Gunten, 2012). To increase the abatement of micropollutants either the ozone exposure or the concentration of hydroxyl radicals needs to be increased in the process. Here, a new technology is needed that can overcome the limitations of bubble columns' mass transfer to improve the MP abatement by ozonation processes.

However, with increasing ozone exposure that could be realized with new technologies for mass transfer, the unfavorable formation of by-products increases in the ozonation process simultaneously. Background organic matter (BOM) and inorganic compounds, i.e., bromide, react with ozone or hydroxyl radicals to potentially harmful oxidation by-products (Krasner et al., 1993; Sohn et al., 2004; Tay et al., 2013). A reaction of particular concern is the oxidation of harmless bromide to carcinogenic bromate (Soltermann et al., 2016; Hübner et al., 2016). Bromide can react directly with ozone or indirectly with hydroxyl radicals to bromate (Hassan et al., 2003). The main parameters affecting bromate formation during ozonation are the pH value, bromide concentration, and ozone dosage (Pinkernell and von Gunten, 2001; Soltermann et al., 2017). Different strategies to limit bromate formation in ozonation have been reported in the literature. Joshi et al. (2020) give an overview of these methods, all of them aiming at lower local ozone concentrations, thus avoiding ozone hotspots, by promoting the ozone decay to hydroxyl radicals. Furthermore, hydrogen peroxide can be added to the wastewater in addition to ozone (Staehelin and Hoigne, 1982; Katsoyiannis et al., 2011). H_2O_2 promotes the decay of ozone to hydroxyl radicals, lowering the concentration of ozone but providing radicals for the degradation of MP. Therefore, this method decreases bromate formation and can increase MP degradation at the same time. Similar strategies to control bromate formation were developed with the addition of chlorine and ammonia (Buffle et al., 2004) or metal catalysts (Andreozzi et al., 1992). However, enhanced hydroxyl radical concentrations can also increase bromate formation during the ozonation process, depending on the water matrix (Gottschalk, 2009). Furthermore, the ozonation process becomes more complex as a result of the necessary addition of chemicals. Therefore, the development of an improved process alternative without additional process steps is favorable.

To overcome both major drawbacks of conventional ozonation, a technology is needed that increases micropollutant degradation and decreases bromate formation at the same time. Membrane contactors are a promising technology to achieve this, since they provide a constant and controlled phase boundary between gaseous ozone and wastewater (Bein et al., 2020). A membrane contactor dissolves ozone bubble-free in the water by diffusive mass transfer through the membrane, thus resulting in custom and controlled mass transfer processes without foaming and very precise reaction conditions (Jansen et al., 2005; Merle et al., 2017; Schmitt et al., 2022). However, this technology has the drawback of increased investment costs. Thus, this technology must significantly improve process performance and operational costs to make it a feasible process alternative. Porous and non-porous membranes are both suitable for membrane contactors for ozonation (Jansen et al., 2005; Berry et al., 2017; Kämmler et al., 2022). To increase the transport of ozone to the bulk phase, the resistance of the liquid side to mass transfer needs to be reduced (Schmitt et al., 2022). Turbulence promoters can be used to create a secondary flow with velocity components perpendicular to the surface of the membrane, reducing the resistance to liquid mass transfer. Therefore, ozone hotspots on the membrane surface can be avoided and a homogeneous concentration of dissolved ozone can be obtained (Sabelfeld and Geißen, 2019). Secondary flow can be created by the geometry of the membrane itself (Jani et al., 2011; Lehmkuhl et al., 2018; Tepper et al., 2022a) or by adding turbulence promoters as an additional part to the membrane contactor (Tepper et al., 2022b). Tepper et al. (2023) were able to show enhanced gas-liquid mass transfer and visualize secondary flow regimes by adding turbulence promoters to the inside channel (lumen side) of a hollow-fiber membrane. Nevertheless, adding turbulence promoters increases the pressure drop in the membrane contactor. Hence, the process improvement regarding bromate formation and micropollutant degradation must be significant to justify the possibly increasing operational costs.

Due to their favorable surface area to volume ratio, tubular membrane contactors are preferred over flat sheet contactors to minimize the footprint of the ozonation reactor (Bein et al., 2020; Bazhenov et al., 2018; Gabelman and Hwang, 1999). Different phase configurations are possible in a tubular membrane contactor. Many studies focus on configurations with the liquid phase on the lumen side and the gas phase on the shell side of the membrane. However, it has also been reported that tubular configuration with gas phase in membrane lumen may have advantages due to less membrane fouling in the narrow lumen channel and possibly better oxidation results as reported by Wen-

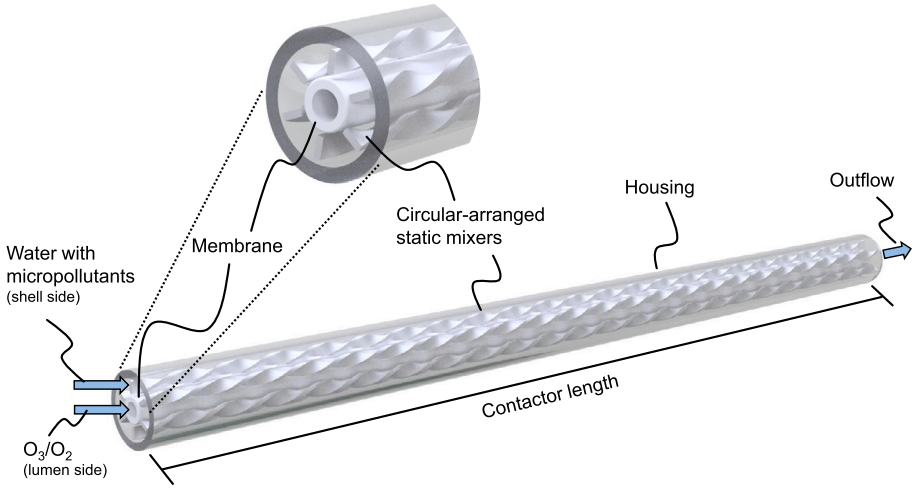

Fig. 1. Rendering of the tubular membrane contactor with six circular-arranged static mixers.

ten et al. (2012). Schmitt et al. (2022, 2023) studied this configuration in single-fiber and multi-fiber contactors with a 3D computational fluid dynamics (CFD) simulation and concluded the importance of mixing within the membrane contactor for an efficient process.

This work presents an ozonation process that uses a membrane contactor for ozonation instead of a bubble column. With this technology, the major drawbacks of conventional ozonation can be diminished. A tubular, porous, hydrophobic membrane is used as a phase boundary between gaseous ozone and water. The hydrophobic property of the membrane ensures gas-filled pores that result in negligible resistances to mass transfer for the gaseous side and the membrane itself (Gabelman and Hwang, 1999). The mass transfer is thus mainly limited by the resistance to mass transfer in the liquid phase. To optimize membrane contactors for ozonation, in this work the mass transfer and distribution of dissolved ozone in wastewater are simulated, and the mass transfer resistance in the liquid channel of a membrane contactor is optimized by lowering the diffusional resistance in the liquid side boundary layer around the membrane by adding turbulence promoters.

Three hypotheses are to be proved within this work. First, it is feasible to avoid ozone hotspots by using membrane contactors with static mixers. Second, bromate formation can be reduced by avoiding ozone hotspots. Third, micropollutant degradation is enhanced by membrane contactors with static mixers. To study the local ozone concentration, bromate formation, and micropollutant abatement in a membrane contactor in detail with high local resolution, a CFD model is developed.

2. Material and methods

In this work, a tubular membrane contactor for ozonation of wastewater is studied. First, the geometry and dimensions of this contactor are presented. Subsequently, the simulation model used to study the membrane contactor, the reaction modeling, further simulation parameters, and strategies to reduce the computational effort are presented.

2.1. Membrane contactor

The membrane contactor consists of a tubular housing, a tubular membrane, and optional static mixers. The gaseous and liquid phases flow on the lumen and shell sides of the membrane, respectively. For all simulations, only the effective membrane length is studied, and the inflow effects of the housing are neglected. Furthermore, the membrane is assumed to be porous and hydrophobic, and all pores are gas filled. To enhance mass transfer, six static mixers are added to the contactor, circularly arranged around the membrane. Fig. 1 shows the geometry of the membrane contactor studied with the dimensions listed in Table 1.

Table 1
Geometry parameters of the simulated membrane contactor.

Membrane contactor		
Lumen diameter	6.0	mm
Membrane thickness	2.0	mm
Housing inner diameter	21.0	mm
Contactor length (2D simulations)	460.0	mm
Contactor length (3D simulations)	480.0	mm
Static Mixer		
Tape width	5.0	mm
Material thickness	1.5	mm
Rotation pitch	40.0	mm
Number of static mixers	6	

2.2. CFD simulations

To study the flow and mass transfer phenomena, ozonation properties, bromate formation and micropollutant degradation within the membrane contactor, the finite element software COMSOL Multiphysics 5.6 was used.

Flow phenomena in the membrane contactor are investigated by solving the Navier-Stokes equations for laminar conditions, as the Reynolds number is < 200 for the given geometry and water flow rate. Due to a stationary process, the time-dependent parts are neglected and the fluid is assumed to be incompressible because of velocities significantly lower than the speed of sound. This results in the equations

$$\rho(\mathbf{v}\cdot\nabla)\mathbf{v} = \nabla\cdot(-p\mathbf{I} + \mu(\nabla\mathbf{v} + (\nabla\mathbf{v})^T)) \tag{1}$$

$$\rho\nabla\cdot\mathbf{v} = 0 \tag{2}$$

where ρ is the density, $\mathbf{v}$ the velocity vector, p the pressure and μ the dynamic viscosity.

The mass transfer of species is modeled by the mass balance equations considering the effects of convection, diffusion, and reactions, represented by

$$\frac{\partial c_i}{\partial t} + \nabla\cdot(-D_i\nabla c_i) + \mathbf{v}\cdot\nabla c_i = R_i \tag{3}$$

where c_i is the concentration of the species i, D_i the diffusion coefficient and R_i the reaction rate of species i.

All occurring reactions are first- or second-order elementary reactions. The overall reaction rate, as the sum of the reaction rates of all reactions of a species i is used in the mass balance equation (3).

Reaction modeling This model covers bromate formation, ozone decomposition, micropollutant degradation, and reactions with background organic matter within the membrane contactor.

In this work, two models for bromate formation and the corresponding models for ozone decay were adapted and compared: the model of Westerhoff et al. (1998) and the model of Hassan et al. (2003) including the adaptions of Fischbacher et al. (2015), referred to as Hassan/Fischbacher model. Both models were implemented in 2D axisymmetric simulations. To model the ozone decay to hydroxyl radicals the Hoigné-Staehelin-Bader (HSB) model by Staehelin et al. (1984) and the Tomiyasu-Fukutomi-Gordon (TFG) model by Tomiyasu et al. (1985) are used in the bromate formation model of Westerhoff and Hassan/Fischbacher, respectively. Both models use the reaction rate constants of Chelkowska et al. (1992).

Furthermore, a simple reaction model for micropollutant degradation was used to investigate the degradation rate and the influence on bromate formation as an ozone sink. The reaction rates of various micropollutants with ozone and hydroxyl radicals have been investigated in literature (Mathon et al., 2021). The hydroxyl radical reaction rates are in the order of $5 \cdot 10^8\,\mathrm{L\,mol^{-1}\,s^{-1}}$ to $1 \cdot 10^{10}\,\mathrm{L\,mol^{-1}\,s^{-1}}$ for a large group of micropollutants (Lee et al., 2013). However, the reaction rates of MPs with ozone are significantly lower and highly dependent on the MP, ranging from $1\,\mathrm{L\,mol^{-1}\,s^{-1}}$ to $1 \cdot 10^6\,\mathrm{L\,mol^{-1}\,s^{-1}}$. Thus, Lee et al. (2013) proposed a classification of MPs into five groups, dependent on their reaction kinetics with ozone and hydroxyl radicals. This work chose to investigate the degradation of a medium-oxidizable micropollutant with an ozone reaction rate constant of $1 \cdot 10^3\,\mathrm{L\,mol^{-1}\,s^{-1}}$ and a low-oxidizable micropollutant with an ozone reaction rate constant of $0.05\,\mathrm{L\,mol^{-1}\,s^{-1}}$. For a maximum ratio of hydroxyl radicals to ozone concentration of $R_{ct} = 5 \cdot 10^{-8}$ that is observed in this study in 2D simulations, the reaction rate of the micropollutants with ozone is one order of magnitude higher than the reaction rate with hydroxyl radicals. Hence, the MP degradation reaction with hydroxyl radicals is neglected to reduce complexity of the model and reactions (4) and (5) are implemented in the reaction model.

$$\mathrm{MP + O_3 \longrightarrow prod} \qquad k_{\mathrm{med}} = 1 \cdot 10^3\,\mathrm{L\,mol^{-1}\,s^{-1}} \tag{4}$$

$$k_{\mathrm{low}} = 0.05\,\mathrm{L\,mol^{-1}\,s^{-1}} \tag{5}$$

Besides micropollutants, the presence of background organic matter in the reactor influences the decomposition of ozone as an initiator, promoter, inhibitor, and in a direct reaction with ozone. A simplified model for this reaction mechanism is implemented with equations (6), (7), (8), and (9), respectively.

$$\mathrm{O_3 + BOM \longrightarrow OH^\bullet + BOM} \qquad k = 7.2\,\mathrm{L\,mol^{-1}\,s^{-1}} \tag{6}$$

$$\mathrm{OH^\bullet + BOM \longrightarrow O_2^{\bullet -} + BOM} \qquad k = 9.72 \cdot 10^8\,\mathrm{L\,mol^{-1}\,s^{-1}} \tag{7}$$

$$\mathrm{OH^\bullet + BOM \longrightarrow BOM} \qquad k = 4.68 \cdot 10^7\,\mathrm{L\,mol^{-1}\,s^{-1}} \tag{8}$$

$$\mathrm{O_3 + BOM \longrightarrow BOM} \qquad k = 2.88\,\mathrm{L\,mol^{-1}\,s^{-1}} \tag{9}$$

Seasonal, geographical and local variations impact the composition of the BOM (Shin et al., 2016). Even though there are no overall valid reaction rates (von Gunten, 2003), Yong and Lin (2013) suggested a way to determine the reaction rates for the four reactions and calculated the rates for three BOM isolates including humic acids and fulvic acids, which are used in this study.

Furthermore, this study uses a constant neutral pH of 7, which is why no buffer is considered. The influence of carbonates on ozone decomposition in the presence of other reactive species, i.e., bromide, was studied in 0D time-dependent simulations and found to be 1% in the relevant time frame of $\ll 5$ min for this study. Thus, carbonate species are not modeled. All reactions used in this work and their reaction rates are described in the SI. The final simulations, with the results presented in this work, were carried out with an adaption of the model of Hassan et al. (2003) and Fischbacher et al. (2015) using the TFG model for the decay of ozone.

For 3D simulations, the reaction model needs to be simplified by only implementing the main reaction pathway in these simulations to limit computational complexity and to be able to solve the reaction model with the given computational resources.

$$\mathrm{Br^- + O_3 \longrightarrow HOBr + O_2} \qquad k = 160\,\mathrm{L\,mol^{-1}\,s^{-1}} \tag{10}$$

$$\mathrm{HOBr + O_3 \longrightarrow BrO_2^- + O_2} \qquad k = R_{ct} \cdot 2 \cdot 10^9\,\mathrm{L\,mol^{-1}\,s^{-1}} \tag{11}$$

$$\mathrm{BrO_2^- + O_3 \longrightarrow BrO_3^- + O_2} \qquad k = 1 \cdot 10^5\,\mathrm{L\,mol^{-1}\,s^{-1}} \tag{12}$$

$$\mathrm{2\,O_3 \longrightarrow 3\,O_2} \qquad k = R_{ct} \cdot 5 \cdot 10^8\,\mathrm{L\,mol^{-1}\,s^{-1}} \tag{13}$$

Instead of modeling the concentration of the hydroxyl radical, this model uses a constant relationship between the hydroxyl radicals and the ozone, the R_{ct} introduced by Elovitz and von Gunten (1999). This work uses a constant R_{ct} of $1 \cdot 10^{-8}$ for 3D simulations. The decomposition of ozone is modeled by Equation (13). The reaction rate constant is adapted from reaction (S1.6). The major part of ozone is decomposed in the radical chain mechanism and with constant R_{ct} the concentration of both educts is known. This results in a second-order reaction of ozone, with two consumed ozone molecules per radical chain.

Furthermore, a reduced bromate formation model is used. In reaction (10) a direct reaction to the hypobromous acid is assumed due to the fast dissociation reaction of the hypobromous acid at pH 7. The reaction rate constant is adapted from (S1.20). The reaction (11) and the reaction rate constant are adapted from (S1.35). The fast reaction of $\mathrm{BrO^\bullet}$ to $\mathrm{BrO_2^-}$ is included in this reaction. The last reaction (12) is adapted from reaction (S1.24). This results in a model with 6 variables instead of 25 and 4 reactions instead of 64. For the modeling of MP degradation reactions (4) and (5) are added to the model.

Simulation domain and parameters Three different model domains are used in this work. A 0D time-dependent simulation model is used to validate the reaction models. For simulations without static mixers a stationary 2D axisymmetric simulation domain can be used, as the tubular membrane contactor is axisymmetric. This significantly decreases the computational effort to solve the model. To simulate static mixers, a stationary 3D model is necessary, as the resulting reactor geometry is not axisymmetric.

Furthermore, to reduce model complexity, the gaseous phase and the membrane are not modeled. Therefore, the concentration gradients in these domains are neglected. The assumption of a negligible mass transfer resistance of the membrane for gas filled pores was proven by Schmitt et al. (2022), where the membrane resistance is less than 1% of the total mass transfer resistance. To model the mass transfer of ozone, an inflow of oxygen and ozone is added at the interface between the membrane and the liquid phase. Table 2 lists the relevant material properties and process parameters for the simulation domain.

To reduce computational effort, the simulation of flow and mass transfer is divided into two steps. In the first step, the velocity field is simulated. In a second step, mass transfer with reaction modeling is simulated based on the resulting velocity field. Furthermore, the simulation domain is divided in axial direction: the geometry is cut into n repeating sections, named periodic elements (PEs), as shown in Fig. 2. The liquid inflow is the inflow of the first PE. The outflow of the first PE is the inflow of the second PE, etc. Every PE has an additional inflow of ozone and oxygen through the membrane interface. The length of a PE results from the total length of the membrane contactor L and the number of PEs used in the simulation. Here, the membrane contactor geometry is cut into 92 PEs with 5 mm per PE for the 2D axisymmetric model and 12 to 24 PEs with 40 mm to 20 mm per PE, respectively, for the 3D model. The length of the PEs needs to match the repeating units of the static mixer geometry, to ensure a continuous static mixer shape. Thus, the length of the membrane contactor in 3D simulations differs slightly from 2D axisymmetric simulations, as shown in Table 1. The simulation

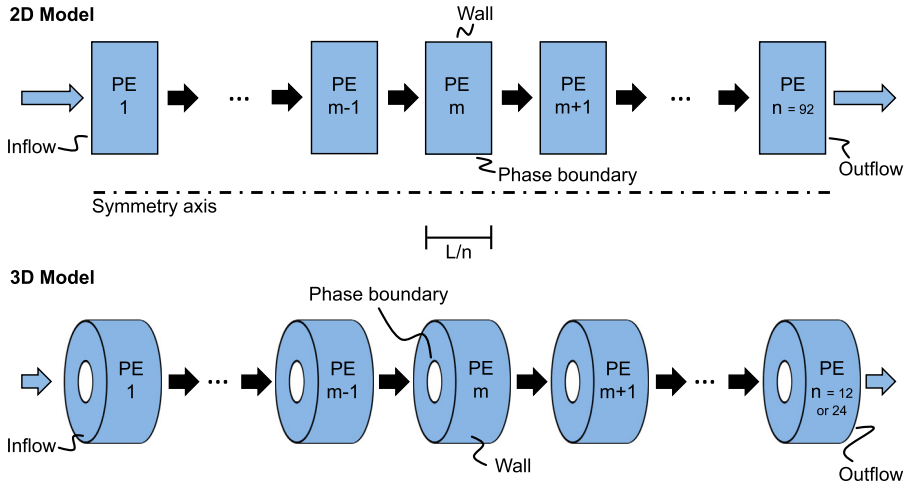

Fig. 2. Simulation domain for the 2D axial symmetric model and the 3D model. The model is divided in axial direction into periodic elements (PEs) in COMSOL Multiphysics.

Table 2
Process parameters of the membrane contactor simulation. Henry coefficients are used in the form of Henry solubility calculated with the ratio of liquid to gas concentration.

Process parameter	Value	Unit			Ref.
Liquid inflow rate	180.00	$mL\,min^{-1}$			
Liquid outflow pressure	110.00	kPa			
Gaseous ozone concentration	4.94	$mol\,m^{-3}$	0.24	$g\,L^{-1}$	
Gaseous oxygen concentration	48.35	$mol\,m^{-3}$	1.55	$g\,L^{-1}$	
Bromide inflow concentration	$1.25 \cdot 10^{-3}$	$mol\,m^{-3}$	100	$\mu g\,L^{-1}$	(Brückner et al., 2018)
MP inflow concentration	$1.00 \cdot 10^{-3}$	$mol\,m^{-3}$			
BOM inflow concentration	$2.50 \cdot 10^{-1}$	$mol\,m^{-3}$			
Henry coefficient ozone $\left(H^{cc}_{S,O_3}\right)$	$2.90 \cdot 10^{-1}$	-			(Sander, 2023)
Henry coefficient oxygen $\left(H^{cc}_{S,O_2}\right)$	$3.20 \cdot 10^{-2}$	-			(Sander, 2023)
Diffusion coefficient ozone	$1.76 \cdot 10^{-9}$	$m^2\,s^{-1}$			(Johnson and Davis, 1996)
Diffusion coefficient oxygen	$2.03 \cdot 10^{-9}$	$m^2\,s^{-1}$			(Xing et al., 2014)
Diffusion coefficient other species	$1.00 \cdot 10^{-9}$	$m^2\,s^{-1}$			

is solved consecutively for the PEs from the membrane contactor's inlet to outlet. The model partition into PEs ensures higher resolutions of the mesh while reducing computational complexity resulting in a 92-fold (2D) respectively 12-fold to 24-fold (3D) lower number of mesh elements per simulations compared to the total model.

The mesh, the polynomial of the shape function, and the length of a PE influence the discretization of the model. For the 2D axisymmetric model the chosen parameters are: $1 \cdot 10^4$ mesh elements per PE, a square shape function for the simulation of the fluid flow and mass transfer, and a PE length of 5 mm. For the 3D model the chosen parameters are: $5 \cdot 10^6$ mesh elements per PE, a linear shape function, and a PE length of 40 mm or 20 mm. A detailed mesh independency study can be found in the SI section S2.1.

All simulations were run on a high performance computing (HPC) cluster of RWTH Aachen University. Each node is equipped with two Intel Xeon Platinum 8160 "SkyLake" Processors (24 cores each) and 192 GB memory.

3. Results and discussion

Both reaction models are validated with experimental data from literature, and a reaction model for all further simulations is selected. With this model, ozonation, MP degradation, bromate formation, and the influence of static mixers in the membrane contactor are studied.

3.1. Simulation model

The reaction models of Westerhoff et al. (1998) and Hassan et al. (2003) including the adaptions of Fischbacher et al. (2015) with the respective ozone decomposition models were first implemented at neutral pH in a 0D time-dependent simulation with a dissolved ozone start concentration of $125 \cdot 10^{-3}\,mol\,m^{-3}$ in water without MPs and BOM. These simulations represent a batch reactor and neglect mass transfer and flow phenomena for a first validation of the reaction models. The simulation results were compared with data from the literature on ozone decomposition and bromate formation in ultrapure water from Westerhoff et al. (1998). Fig. 3 a) shows the concentration of ozone over time without bromide in water. Compared to experimental data, the Hassan/Fischbacher model slightly overpredicts the ozone concentration in the first 25 min. However, the Westerhoff model fits the experimental data very well in the first 20 min and slightly overpredicts the ozone concentration afterwards. However, both simulation models agree well with the experimental data. Fig. 3 b) shows the ozone concentration over time in the presence of bromide with a start concentration of $5 \cdot 10^{-3}\,mol\,m^{-3}$. As a result of the reaction of bromide with hydroxyl radicals the concentration of hydroxyl radicals is reduced, leading to a slower overall ozone decomposition than in the absence of bromide. Both simulation models represent this behavior in good agreement with the experimental data. The Hassan/Fischbacher model fits the experimental data better, while the Westerhoff model underpredicts the ozone concentration for the whole time range of the simulation.

The formation of bromate at neutral pH with an ozone start concentration of $62.5 \cdot 10^{-3}\,mol\,m^{-3}$ of both models is shown in Fig. 3 c).

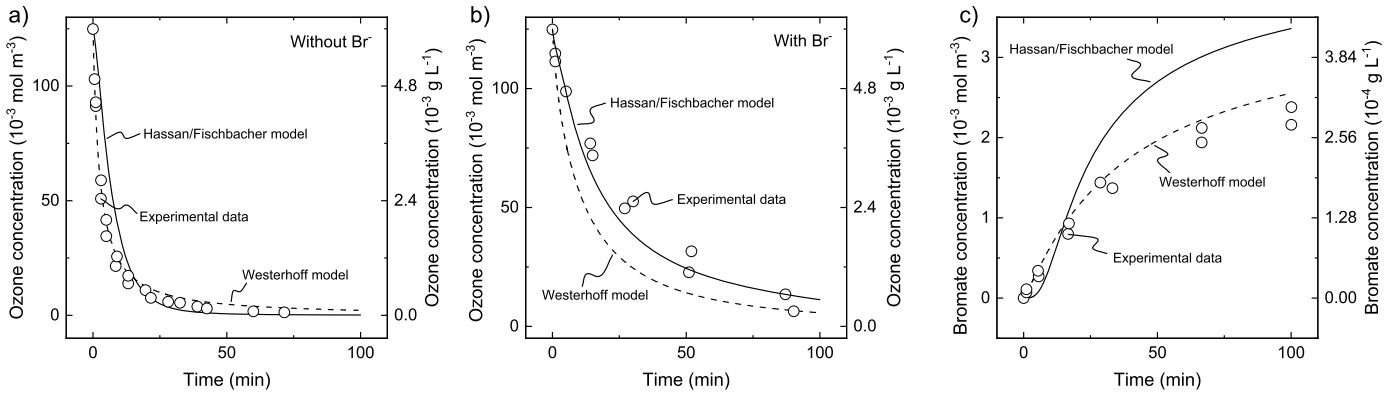

Fig. 3. Comparison of experimental data from Westerhoff et al. (1998) to the ozone decay and bromate formation models of Westerhoff et al. (1998) and Hassan et al. (2003) including the adaptions of Fischbacher et al. (2015) in a 0D time-dependent simulation. a) Ozone concentration in the absence of bromide with an initial ozone concentration of $125 \cdot 10^{-3}$ mol m^{-3}. b) Ozone concentration in the presence of bromide with an initial ozone concentration of $125 \cdot 10^{-3}$ mol m^{-3} and initial bromide concentration of $5 \cdot 10^{-3}$ mol m^{-3}. c) Bromate formation over time with an initial ozone concentration of $62.5 \cdot 10^{-3}$ mol m^{-3} and initial bromide concentration of $5 \cdot 10^{-3}$ mol m^{-3}.

Compared to the experimental data of Westerhoff et al., the model of Hassan/Fischbacher slightly underestimates the bromate concentration in the first 20 min and overpredicts it thereafter. The model of Westerhoff slightly overpredicts the bromate formation over the entire time range of the simulation. Both models seem suitable for an estimation of bromate formation during ozonation. However, an overprediction of bromate formation by the model is favored over an underprediction for later process and reactor design.

Then both models were implemented in stationary 2D simulations including mass transfer and fluid flow using the membrane contactor geometry without static mixers. Concentrations of ozone and bromate throughout the membrane contactor are shown in Fig. 4 a) and b), respectively. The ozone concentration in the contactor drops for both reaction models compared to the sole ozone input without reactions due to ozone consumption by bromate formation. This effect increases the concentration gradient between the gaseous and aqueous phases, enhancing ozone mass transfer. In the literature, reaction models often describe this with an enhancement factor (Schmitt et al., 2022; Bein et al., 2020). Here, we model the effect rigorously in this work through to the explicit reaction model. The ozone concentration at the membrane contactor outlet is 40% lower for the Westerhoff model compared to the Hassan/Fischbacher model. However, the bromate concentration at the contactor outlet is 39% higher using the Hassan/Fischbacher model compared to the Westerhoff model.

As an overprediction in bromate formation is preferred over an underprediction for reactor and process design, the Hassan/Fischbacher model with the TFG model for ozone decay was used for all subsequent simulations.

The reduced bromate formation model developed in this work, consisting of equations (10) to (13), was also validated in a time-dependent 0D simulation with experimental data from Westerhoff et al. (1998). Ozone and bromate concentrations over time are shown in Fig. 5 a) and b), respectively. Although the ozone decay is in good agreement with experimental data, the bromate formation is significantly overpredicted with the reduced model for long residence times. However, without simplifying the model, a 3D simulation of the membrane contactor with reactions is impossible even with the presented model partitioning due to the limited memory of 192 GB per node on the HPC cluster used. Furthermore, residence times in the membrane contactor are below 1 min and, compared to the time range of the 0D simulations, very low, limiting the overprediction of bromate formation. Thus, the reduced model is used for 3D simulations, and an overprediction of the bromate concentration is accepted to get a conservative estimation of the bromate formation in the membrane contactor.

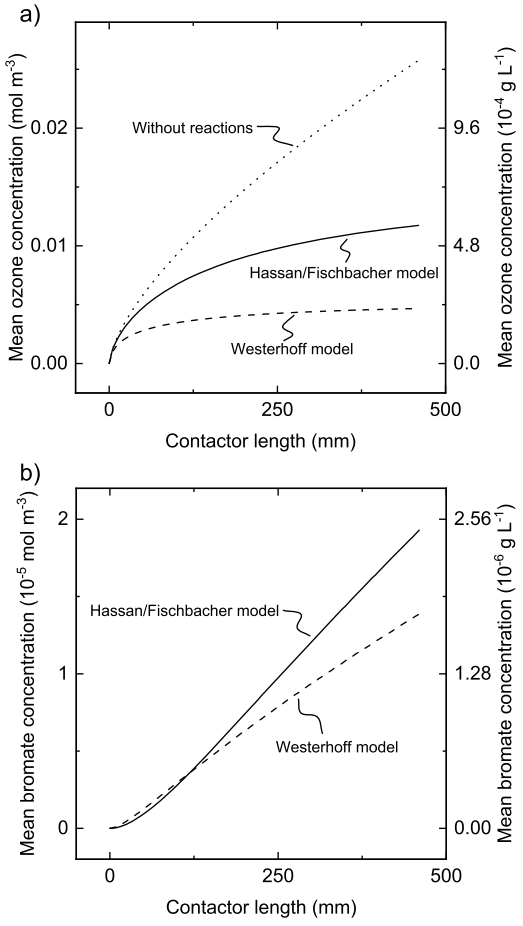

Fig. 4. Comparison of the reaction models by Hassan et al. (2003) including the adaptions of Fischbacher et al. (2015) and Westerhoff et al. (1998) in a 2D simulation of the membrane contactor. a) Mean ozone concentration over the contactor length. b) Mean bromate concentration over the contactor length.

3.2. Ozonation with membrane contactors

Simulations were performed to study the ozonation behavior of the membrane contactor. In the absence of static mixers, the 2D rotational symmetric domain with the full reaction model is used. In the presence of static mixers, 3D simulations are necessary to implement static mixers in the geometry. These simulations use the reduced reaction model.

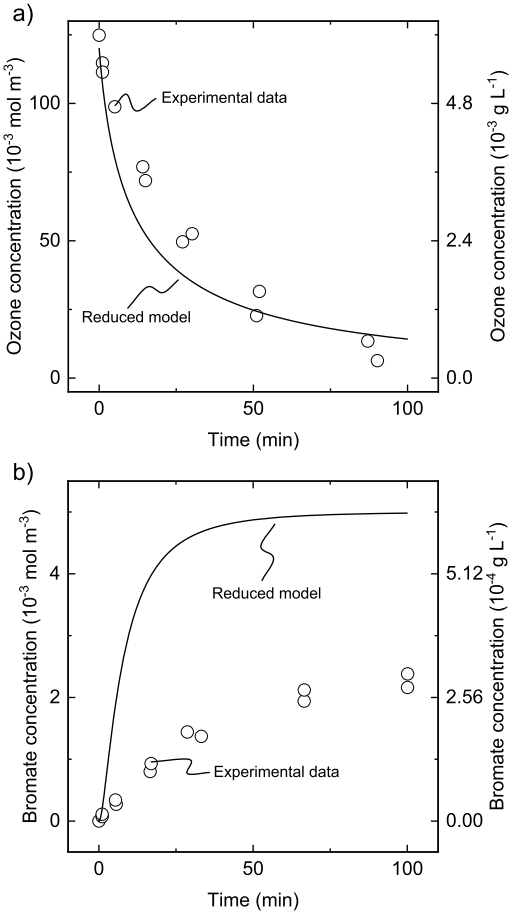

Fig. 5. Comparison of the reduced reaction model in a 0D time-dependent simulation to experimental data from Westerhoff et al. (1998). a) Ozone concentration in the presence of bromide with an initial ozone concentration of $125 \cdot 10^{-3}$ mol m^{-3} and initial bromide concentration of $5 \cdot 10^{-3}$ mol m^{-3}. b) Bromate formation over time with an initial ozone concentration of $62.5 \cdot 10^{-3}$ mol m^{-3} and initial bromide concentration of $5 \cdot 10^{-3}$ mol m^{-3}.

The reaction model serves as a sink for ozone in water; thus, no further artificial enhancement factor for ozone mass transfer is needed in the simulation, as the enhancement effect is modeled rigorously. Fig. 6 b) shows the concentration of ozone in water in the cross section of the membrane contactor outlet without static mixers. The ozone concentration is high at the membrane's surface and decreases strongly toward the bulk phase. A boundary layer with high concentrations of ozone is formed around the membrane. This can be explained by the flow conditions without radial flow components at Re = 120 inside the membrane contactor. Therefore, the transfer of ozone is limited in the radial direction to diffusion only, and the bulk phase with higher distances from the membrane has an ozone concentration of 0 mol m^{-3}.

Due to the formation of an ozone boundary layer and diffusive mass transfer in the radial direction, the overall mass transfer of ozone from gas to liquid is low. Fig. 6 a) shows the ozone flux through the membrane for every periodic element of the membrane contactor. The ozone flux without static mixers starts at $25.4 \cdot 10^{-6}$ mol m^{-2} s^{-1} for the first periodic element with a length of 5 mm and decreases significantly within the first 40 mm to$11.8 \cdot 10^{-6}$ mol m^{-2} s^{-1}. The steep slope shows the fast saturation of the boundary layer with ozone. During the saturation process, the concentration gradient between the gas and liquid phase decreases. This being the driving force of mass transfer in the membrane contactor, the mass transfer of ozone through the membrane decreases over the contactor length. The ozone flux faces a lower threshold with increasing contactor length of $10.2 \cdot 10^{-6}$ mol m^{-2} s^{-1}. After saturation of the boundary layer, the ozone flux is mainly driven by the consumption of ozone in the boundary layer due to reactions. Thus, the total flow of ozone through the membrane is limited to $1.56 \cdot 10^{-7}$ mol s^{-1} for a membrane contactor without static mixers.

To overcome the limited mass transfer, circular-arranged static mixers are added to the flow channel between the membrane and the housing, creating a convective flow in radial direction. Fig. 6 c) shows the concentration of ozone in water in the outlet cross section of the membrane contactor with static mixers. The ozone concentration at the membrane's surface is still high with a maximum of 1.4 mol m^{-3}, which is higher than the bulk phase concentration. However, the concentration in the bulk phase increased significantly with the addition of static mixers, to a value of 0.05 mol m^{-3} or higher.

The concentration gradient between the gas and liquid phase is more even over the length of the contactor, resulting in a constant driving force for ozone mass transfer. Compared to the membrane contactor without static mixers, the ozone flux is significantly increased, as can be seen for the contactor with static mixers in Fig. 6 a). Using static mixers, the ozone flux faces a lower threshold of $17.8 \cdot 10^{-6}$ mol m^{-2} s^{-1}, which is 75% higher compared to the contactor without static mixers. The total flow of ozone through the membrane increases to $2.78 \cdot 10^{-7}$ mol s^{-1}, which is an increase of 78%.

Furthermore, the mass transfer coefficient (K_L) can be calculated for both contactor configurations. Therefore, simulations without reactions were used to study sole mass transfer. The K_L value of the contactor without static mixers is $1.09 \cdot 10^{-5}$ m s^{-1} and it increases to $1.79 \cdot 10^{-5}$ m s^{-1} when static mixers are added. Due to the convective transport of ozone into the bulk phase, the liquid phase mass transfer resistance is lowered and the K_L is significantly increased by static mixers. In general, the K_L value for ozone increases by 64% by adding static mixers into the membrane contactor.

In comparison, Schmitt et al. (2022) observed a K_L of $4.789 \cdot 10^{-5}$ m s^{-1} at Re = 400 in a tubular polytetrafluoroethylene (PTFE) membrane contactor in lab-scale ozonation experiments. Water was applied on the shell side of the membrane module, as in the simulations of this work. However, the Reynolds number is significantly higher compared to this work, where Re is only 30% of the value of Schmitt et al. The results of this work for K_L are in the same order of magnitude. However, the simulations with static mixers reach only 37% of the K_L value determined by Schmitt et al. This can be explained by the difference in Reynolds number, as mass transfer is improved with increasing Re, shown by (Pines et al., 2005). They found a nearly linear correlation between the Reynolds number and mass transfer coefficient for all membrane materials tested for Re between 60 and 2000 (Pines et al., 2005). Hence, it is expected that K_L values in our simulations are below the values of Schmitt et al. Taking this effect into account, the simulation results are in good agreement with their experimental results. Furthermore, the increase of K_L by increasing the Reynolds number, as described by Pines et al., is in agreement with the increase in K_L in simulations with static mixers within this work, as static mixers have the same effect of lowering the resistance to liquid side mass transfer resistance as an increase in Reynolds number.

3.3. Micropollutant degradation in membrane contactors

The degradation of a low-oxidizable and a medium-oxidizable micropollutant with reaction rate constants of 0.05 L mol^{-1} s^{-1} and $1 \cdot 10^3$ L mol^{-1} s^{-1}, respectively, were studied in the membrane contactor in the absence and presence of static mixers. The ozone dosage in these simulations, according to Section 3.2, is 52 mol_{O_3} mol_{MP}^{-1} and 92 mol_{O_3} mol_{MP}^{-1} for 2D and 3D simulations, respectively. Fig. 7 a) reveals the strong influence of radial mixing and more equal ozone distribution within the reactor volume on the degradation of a medium-oxidizable micropollutant. The membrane contactor without static mixers shows a linear decrease of the radial averaged micropollutant concentration over the membrane contactor length for both micropollutants. However, the low-oxidizable micropollutant shows no significant

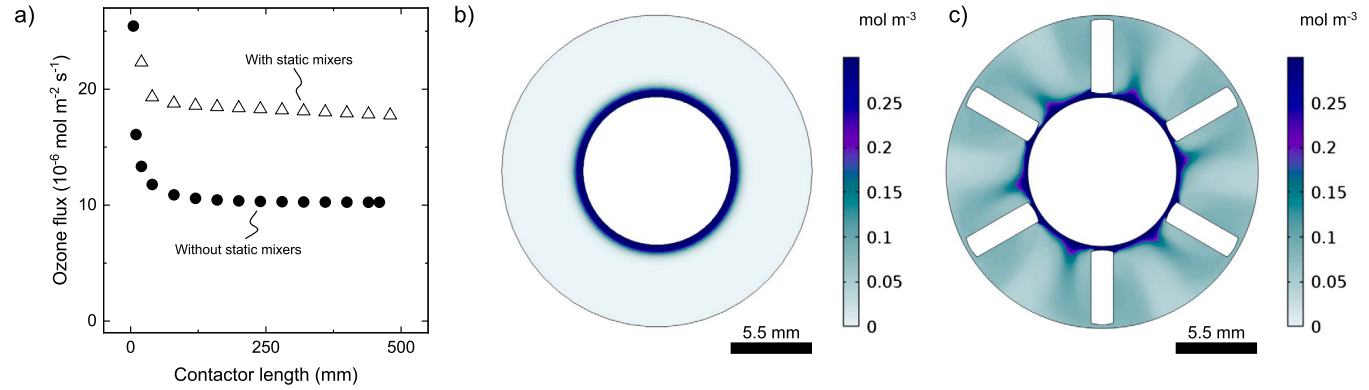

Fig. 6. Simulations of the membrane contactor with and without static mixers. a) Ozone flux through the membrane for each periodic element over the length of the contactor (without static mixers, only selected PEs are shown). b) Ozone concentration at the outlet in absence of static mixers. c) Ozone concentration at the outlet in presence of static mixers.

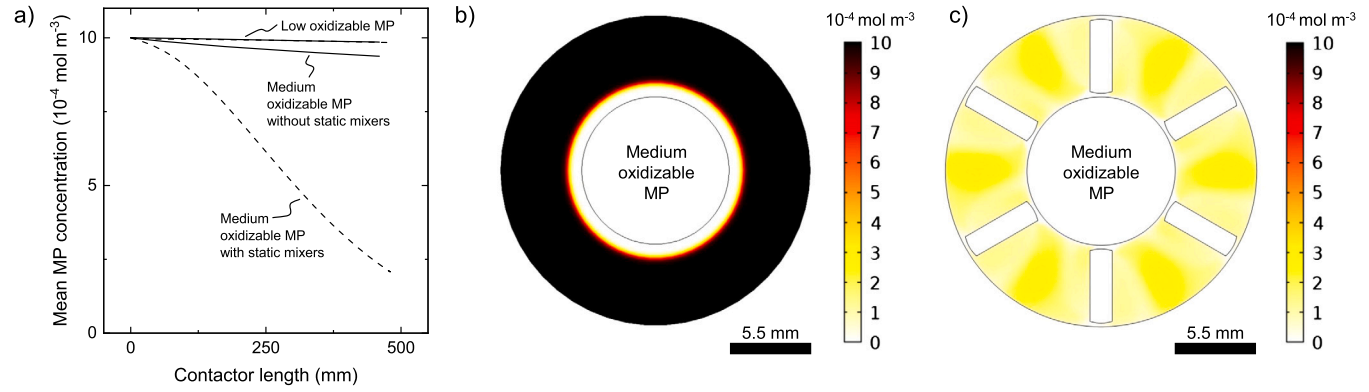

Fig. 7. Simulation of the membrane contactor with and without static mixers. a) Mean concentration of a low-oxidizable and medium-oxidizable micropollutant over the contactor length. b) Concentration of a medium-oxidizable micropollutant at the outlet in absence of static mixers. c) Concentration of a medium-oxidizable micropollutant at the outlet in presence of static mixers.

degradation due to the slow reaction rate. Fig. 7 b) shows the concentration of the medium-oxidizable micropollutant in the radial cross section at the contactor outlet. In the bulk phase of the contactor, no degradation of micropollutants occurs due to the absence of ozone, as shown in Fig. 6 b). Thus, the degradation of micropollutants is limited to the boundary layer around the membrane. Because of the small volume of the boundary layer compared to the bulk phase, the overall degradation of a medium-oxidizable micropollutant is limited to 6 %. However, in areas of high ozone concentration around the membrane, the medium-oxidizable micropollutant is completely degraded.

In contrast, the degradation of a medium-oxidizable micropollutant is significantly enhanced by the implementation of static mixers in the membrane contactor. The micropollutant concentration decreases significantly throughout the contactor, as shown in Fig. 7. However, static mixers do not affect the degradation of a low-oxidizable micropollutant. The concentration curves are very similar and not distinguishable in Fig. 7 in the absence and presence of static mixers. This indicates a reaction rate limitation rather than a mass transfer limitation for this micropollutant. Thus, other strategies need to be used to increase the degradation rate for these micropollutants, e.g., increasing the hydroxyl radical concentration with H_2O_2 addition or use of (photo-) catalytic ozonation.

Since the ozone flux remains constant after the inflow peak in this configuration, a high amount of dissolved ozone is present within the contactor to degrade micropollutants. Therefore, the degradation rate of a medium-oxidizable micropollutant is approximately constant until 400 mm contactor length. Here, the concentration of the micropollutant is already decreased by 68 %, and the degradation reaction is starting to be limited by the low concentration of micropollutants, resulting in a decrease in the degradation rate towards the membrane contactor outlet. At the outlet of the contactor with static mixers, the concentration of the medium-oxidizable micropollutant is decreased by 79 %. Fig. 7 c) shows that the whole contactor volume is involved in micropollutant degradation due to the presence of ozone across the entire membrane contactor volume as shown in Fig. 6 c). The concentration of the medium-oxidizable micropollutant is decreased by at least 50 % in all areas of the cross section at the membrane contactor outlet. This indicates the degradation of a medium-oxidizable micropollutant is rather mass transfer limited than reaction rate limited in absence of static mixers and the clear advantage of a membrane contactor equipped with static mixers for medium-oxidizable micropollutant degradation, as already assumed after the evaluation of the ozone distribution within the membrane contactor.

Overall, using static mixers in the membrane contactor results in a 13 times higher degradation of a medium-oxidizable micropollutant with the same process parameters because of higher ozone mass transfer and more equal ozone distribution in the reactor volume.

3.4. Bromate formation in membrane contactors

Fig. 8 shows the mean bromate concentration as a function of the axial position in the membrane contactor in the absence and presence of static mixers. The ozone dosage in these simulations, according to Section 3.2, is 52 $mol_{O_3}\ mol_{MP}^{-1}$ and 92 $mol_{O_3}\ mol_{MP}^{-1}$ for 2D and 3D simulations, respectively. Starting with no bromate at the contactor inlet and a bromide concentration of $1.25 \cdot 10^{-3}$ mol m^{-3}, the bromate concentration in the contactor without static mixers increases almost linearly with the contactor length. Bromate can only be formed in

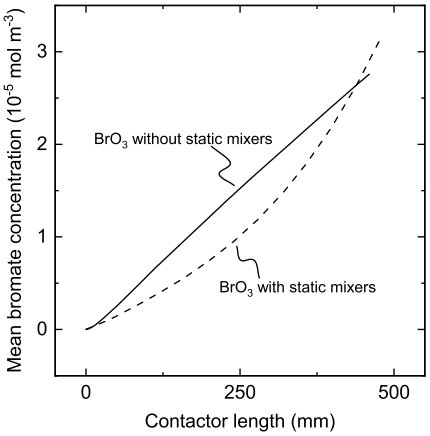

Fig. 8. Mean bromate concentration in presence and absence of static mixers.

the volume around the membrane where dissolved ozone is present, and bromate formation increases with higher ozone concentrations. Thus, bromate formation in the contactor without static mixers is limited to the boundary layer, where ozone is present at high concentrations. The mean bromate concentration at the contactor outlet is $2.75 \cdot 10^{-5}\,\mathrm{mol\,m^{-3}}$ without static mixers. The bromide concentration in the contactor is two orders of magnitude higher; hence, no limitation due to a decrease in bromide concentration is observed here, explaining the linear increase in bromate over the contactor length.

The bromate concentration in the membrane contactor with static mixers behaves differently. In the first part of the membrane contactor, lower mean bromate concentrations are observed. However, the slope of the mean bromate concentration increases with increasing contactor length and becomes larger compared to the contactor without static mixers after approximately 260 mm. After this point, bromate formation is higher in the contactor with static mixers due to the higher concentration of dissolved ozone in the whole cross-sectional area. Thus, the mean bromate concentration exceeds the values of the contactor without static mixers after 440 mm.

After a length of 200 mm, the dissolved ozone concentration in water in the contactor with static mixers is the same as after 460 mm in the contactor without static mixers. Beyond this point, the mean ozone concentrations with static mixers exceed those without static mixers. As a result of the increase in the number of ozone molecules, bromate formation is promoted. Furthermore, ozone is present in the entire volume of the membrane contactor and is not limited to a small volume around the membrane. This leads to bromate formation across the entire reactor volume. These effects explain the increasing slope of bromate concentration over contactor length for the static mixer configuration. A significant increase of bromate formation in membrane contactors at reduced mass transfer limitations was also demonstrated in experiments by Kämmler et al. (2022).

However, in the first part of the contactor, the bromate formation is lower with static mixers, because the slope of the mean bromate formation is lower. This can be explained by a significantly increased radial mass transfer of ozone from the membrane to the bulk phase, resulting in a reduced concentration of ozone in the boundary layer of the membrane. Hence, the bromate formation is reduced by avoiding ozone hotspots around the membrane, although the overall mass transfer of ozone into the liquid phase increases. This effect confirms the hypothesis that bromate formation can be decreased by avoiding ozone hotspots in the membrane contactor. However, the benefit of avoiding ozone hotspots by static mixers is diminished due to a higher overall ozone concentration in the membrane contactor and thus an overall increased bromate formation.

Since the mean ozone concentration at the membrane contactor outlet in the presence of static mixers is still high with $0.09\,\mathrm{mol\,m^{-3}}$, while around 80% of the MPs are already degraded, the gaseous ozone concentration may be lowered to reduce bromate formation. Furthermore, this is a major advantage considering the energy demand of the process. Hence, the gaseous ozone concentration is lowered by 50 % from $4.94\,\mathrm{mol\,m^{-3}}$ to $2.47\,\mathrm{mol\,m^{-3}}$ for 3D simulations with static mixers. Fig. 9 shows the results of these simulations. The total ozone flow through the membrane for the lowered gaseous ozone concentration is $1.33 \cdot 10^{-7}\,\mathrm{mol\,s^{-1}}$, which is a proportional decrease by 50% compared to the high gaseous ozone concentration. This correlation between gaseous ozone concentration and dissolved ozone concentration is in accordance with experimental results (Kämmler et al., 2022).

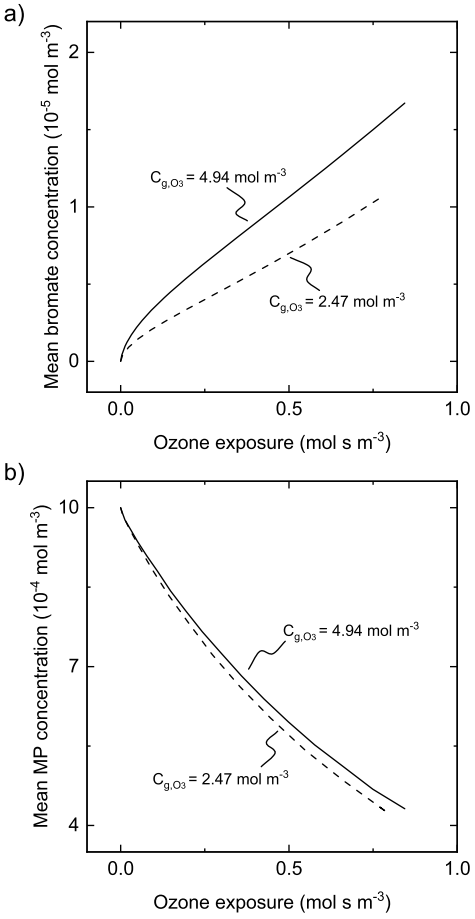

Fig. 9. Variation of the gaseous ozone concentration at the membrane contactor inlet. a) Mean bromate concentration over the ozone exposure for different gaseous ozone concentrations. b) Mean MP concentration for a medium-oxidizable MP over the ozone exposure.

The ozone exposure is used to compare bromate formation as a function of gaseous ozone concentration. The ozone exposure is the product of the concentration of liquid ozone and the time that the individual is exposed to this concentration. Thus, lower gaseous ozone concentrations would be beneficial if less bromate was formed at the same ozone exposures compared to high gaseous ozone concentrations. Here, the ozone exposure is calculated according to equation (S2.3). Higher residence times or contactor lengths are necessary for the same ozone exposure in simulations with lower gaseous ozone concentrations. In this work, we kept the liquid flow rate constant and compared different positions in the membrane contactor for the same ozone exposure at different gaseous ozone concentrations.

Fig. 9 a) shows the mean bromate concentration in the contactor as a function of ozone exposure. A steep increase in bromate concentration for low ozone exposures is observed for both gaseous ozone concentrations, followed by an approximated linear increase. However, for lower gaseous ozone concentrations, the mean bromate concentration is always lower at the same ozone exposure compared to high gaseous

ozone concentrations. At an ozone exposure of $0.78\,\mathrm{mol\,s\,m^{-3}}$, which is reached at the reactor outlet for low gaseous ozone concentration, the mean bromate concentration is 31 % lower for low gaseous ozone concentration. These results are in accordance with experimental results of (Stylianou et al., 2018) and (Kämmler et al., 2022), who demonstrated that lower gaseous ozone concentrations with increased residence times in membrane contactors result in reduced bromate formation and increased micropollutant degradation. Thus, it is concluded that lowering the gaseous ozone concentration is a significant parameter to decrease bromate formation in ozonation processes. Increased ozone mass transfer in the presence of static mixers enables this without reducing the overall ozone flux through the membrane.

Fig. 9 b) shows the micropollutant degradation in the membrane contactor for high and low gaseous ozone concentrations as a function of ozone exposure. The degradation curves for both gaseous ozone concentrations are very similar. However, the micropollutant concentration at lower gaseous ozone concentrations is slightly lower, with an increasing difference to the high gaseous ozone concentration curve for higher ozone exposures. This result indicates that at least the micropollutant degradation is not decreased by using a lower concentration of gaseous ozone at the same ozone exposure due to the increased residence time. However, we do not conclude that an enhancement is present with low gaseous ozone concentrations due to the small difference.

4. Conclusion

A complex simulation model for a tubular membrane contactor was successfully implemented in COMSOL Multiphysics within this work. Fluid dynamics simulations were coupled with mass transfer and reaction simulations for ozonation, ozone decay, micropollutant degradation, reactions with background organic matter, and bromate formation. A simplification of the bromate formation model was developed and implemented in 3D simulations of the membrane contactor in the presence of static mixers. The simulations were validated with experimental data from the literature, and the results are in good agreement with data from the literature for ozonation behavior and bromate formation in 2D axisymmetric simulations. However, the reduced bromate formation model that needed to be used in 3D simulations to reduce mathematical complexity tends to overpredict the bromate formation. Furthermore, a discretization method using periodic elements for the membrane contactor was found. This discretization minimizes the mathematical complexity of the model and enables the simulation of complex mass transfer and reaction phenomena in 2D axisymmetric and 3D simulations. However, the simulation models have limitations due to the need to decrease the number of chemical reactions. The influence of carbonate species and pH are neglected, and the 3D model's overprediction of bromate formation is accepted. Furthermore, the 3D model is not capable of simulating the full ozone decomposition and bromate formation model and needs reduced models. For future work, the 3D model could be improved by increasing computational power or changing the simulation method. Here, finite volume methods may be superior to a finite element method used by COMSOL Multiphysics.

The simulation results demonstrate the importance of radial mixing in tubular membrane contactors for ozonation. The membrane ozone flux can be increased by 75% in the presence of static mixers. Furthermore, the micropollutant degradation benefits from a higher ozone concentration in the liquid phase and can be increased by 13 times compared to a contactor without static mixers.

Furthermore, it is shown that the bromate formation is reduced in the first part of the membrane contactor in the presence of static mixers due to the decreased ozone hotspots around the membrane's surface. In contrast, the bromate formation increases significantly in the second part of the contactor because of a higher dissolved ozone concentration. As the reduced bromate formation model tends to overpredict the bromate formation, this can also contribute to increased bromate formation in the presence of static mixers.

Because of the significantly increased ozone flux in the presence of static mixers, the effect of a decreased gaseous ozone concentration on bromate formation and micropollutant degradation was studied. At the same ozone exposure, the bromate formation is 31% lower when the gaseous ozone concentration is lowered by 50%. This result confirms the hypothesis that ozone hotspots mainly contribute to undesired bromate formation. The effect may even be under-predicted by the results of this work as the bromate formation tends to be over-predicted. At the same time, micropollutant degradation was not affected by lower gaseous ozone concentrations at the same ozone exposure due to the increased residence time.

Nevertheless, the membrane contactor technology with static mixers also has possible drawbacks that need further investigation. Membrane fouling is a potential problem in wastewater ozonation, causing performance losses over time and the necessity for membrane cleaning or replacement. Furthermore, the pressure drop induced by static mixers needs to be studied for an application-relevant reactor size and flow rate, as it increases the power consumption of pumps. Hence, the operational costs need to be compared to the costs of head losses in traditional ozonation systems.

Overall, static mixers enable the use of a lower gaseous ozone concentration by increasing the ozone mass transfer coefficient in the membrane contactor. Thus, they contribute to a decreased bromate formation while the micropollutant degradation is unaffected at the same ozone exposure.

CRediT authorship contribution statement

Stefan Herrmann: Writing – review & editing, Writing – original draft, Visualization, Validation, Methodology, Investigation, Conceptualization. **Maria C. Padligur:** Writing – original draft, Validation, Methodology, Investigation. **Conrad J. Bieneck:** Writing – original draft, Validation, Investigation. **Matthias Wessling:** Writing – review & editing, Supervision, Resources, Funding acquisition, Conceptualization.

Declaration of competing interest

The authors declare that they have no known competing financial interests or personal relationships that could have appeared to influence the work reported in this paper.

Data availability

Data will be made available on request.

Acknowledgements

M.W. acknowledges DFG funding through the Gottfried Wilhelm Leibniz Award 2019 (WE 4678/12-1). Simulations were performed with computing resources granted by RWTH Aachen University under project thes1186.

Appendix A. Supplementary material

Supplementary material related to this article can be found online at https://doi.org/10.1016/j.ces.2024.119924.

References

Altmann, J., Ruhl, A.S., Zietzschmann, F., Jekel, M., 2014. Direct comparison of ozonation and adsorption onto powdered activated carbon for micropollutant removal in advanced wastewater treatment. Water Res. 55, 185–193. https://doi.org/10.1016/j.watres.2014.02.025.

Andreozzi, R., Insola, A., Caprio, V., D'Amore, M.G., 1992. The kinetics of mn(ii)-catalysed ozonation of oxalic acid in aqueous solution. Water Res. 26 (7), 917–921. https://doi.org/10.1016/0043-1354(92)90197-C.

Bazhenov, S.D., Bildyukevich, A.V., Volkov, A.V., 2018. Gas-liquid hollow fiber membrane contactors for different applications. Fibers 6 (4), 76. https://doi.org/10.3390/fib6040076.

Bein, E., Zucker, I., Drewes, J.E., Hübner, U., 2020. Ozone membrane contactors for water and wastewater treatment: a critical review on materials selection, mass transfer and process design. Chem. Eng. J., 127393. https://doi.org/10.1016/j.cej.2020.127393.

Berry, M., Taylor, C., King, W., Chew, Y., Wenk, J., 2017. Modelling of ozone mass-transfer through non-porous membranes for water treatment. Water 9 (7), 452. https://doi.org/10.3390/w9070452.

Brückner, Ira, Stepkes, Hermann, Differding, Michele, 2018. Darstellung der technischen umsetzbarkeit einer verfahrensstufe zur spurenstoffelimination als variantenvergleich auf der kläranlage eilendorf. Machbarkeitsstudie.

Buffle, M.-O., Galli, S., von Gunten, U., 2004. Enhanced bromate control during ozonation: the chlorine-ammonia process. Environ. Sci. Technol. 38 (19), 5187–5195. https://doi.org/10.1021/es0352146.

Chelkowska, K., Grasso, D., Fábián, I., Gordon, G., 1992. Numerical simulations of aqueous ozone decomposition. Ozone Sci. Eng. 14 (1), 33–49. https://doi.org/10.1080/01919519208552316.

El-taliawy, H., Ekblad, M., Nilsson, F., Hagman, M., Paxeus, N., Jönsson, K., Cimbritz, M., La Cour Jansen, J., Bester, K., 2017. Ozonation efficiency in removing organic micro pollutants from wastewater with respect to hydraulic loading rates and different wastewaters. Chem. Eng. J. 325, 310–321. https://doi.org/10.1016/j.cej.2017.05.019.

Elovitz, M.S., von Gunten, U., 1999. Hydroxyl radical/ozone ratios during ozonation processes. I. The r ct concept. Ozone Sci. Eng. 21 (3), 239–260. https://doi.org/10.1080/01919519908547239.

Fischbacher, A., Löppenberg, K., von Sonntag, C., Schmidt, T.C., 2015. A new reaction pathway for bromite to bromate in the ozonation of bromide. Environ. Sci. Technol. 49 (19), 11714–11720. https://doi.org/10.1021/acs.est.5b02634.

Gabelman, A., Hwang, S.-T., 1999. Hollow fiber membrane contactors. J. Membr. Sci. 159 (1–2), 61–106. https://doi.org/10.1016/S0376-7388(99)00040-X.

Gardoni, D., Vailati, A., Canziani, R., 2012. Decay of ozone in water: a review. Ozone Sci. Eng. 34 (4), 233–242. https://doi.org/10.1080/01919512.2012.686354.

Gottschalk, C., 2009. Ozonation of Water and Waste Water: A Practical Guide to Understanding Ozone and Its Applications, 2nd edition. John Wiley & Sons Incorporated, Hoboken. https://ebookcentral.proquest.com/lib/kxp/detail.action?docID=661861.

Hassan, K.Z.A., Bower, K.C., Miller, C.M., 2003. Numerical simulation of bromate formation during ozonation of bromide. J. Environ. Eng. 129 (11), 991–998. https://doi.org/10.1061/(ASCE)0733-9372(2003)129:11(991).

Hübner, U., Kuhnt, S., Jekel, M., Drewes, J.E., 2016. Fate of bulk organic carbon and bromate during indirect water reuse involving ozone and subsequent aquifer recharge. J. Water Reuse Desalination 6 (3), 413–420. https://doi.org/10.2166/wrd.2015.222.

Jani, J.J.M., Wessling, M., Lammertink, R.G., 2011. Geometrical influence on mixing in helical porous membrane microcontactors. J. Membr. Sci. 378 (1–2), 351–358. https://doi.org/10.1016/j.memsci.2011.05.021.

Jansen, R., de Rijk, J.W., Zwijnenburg, A., Mulder, M., Wessling, M., 2005. Hollow fiber membrane contactors - a means to study the reaction kinetics of humic substance ozonation. J. Membr. Sci. 257 (1–2), 48–59. https://doi.org/10.1016/j.memsci.2004.07.038.

Jiang, J.-Q., Zhou, Z., Sharma, V.K., 2013. Occurrence, transportation, monitoring and treatment of emerging micro-pollutants in waste water — a review from global views. Microchem. J. 110, 292–300.

Johnson, P.N., Davis, R.A., 1996. Diffusivity of ozone in water. J. Chem. Eng. Data 41 (6), 1485–1487. https://doi.org/10.1021/je9602125.

Joshi, R., Ratpukdi, T., Knutson, K., Bhatnagar, A., Khan, E., 2020. Bromate formation control by enhanced ozonation: a critical review. Crit. Rev. Environ. Sci. Technol. 52 (7), 1154–1198. https://doi.org/10.1080/10643389.2020.1850169.

Kämmler, J., Zoumpouli, G.A., Sellmann, J., Chew, Y.M.J., Wenk, J., Ernst, M., 2022. Decolorization and control of bromate formation in membrane ozonation of humic-rich groundwater. Water Res. 221, 118739. https://doi.org/10.1016/j.watres.2022.118739.

Kanakaraju, D., Glass, B.D., Oelgemöller, M., 2018. Advanced oxidation process-mediated removal of pharmaceuticals from water: a review. J. Environ. Manag. 219, 189–207. https://doi.org/10.1016/j.jenvman.2018.04.103.

Katsoyiannis, I.A., Canonica, S., von Gunten, U., 2011. Efficiency and energy requirements for the transformation of organic micropollutants by ozone, o3/h2o2 and uv/h2o2. Water Res. 45 (13), 3811–3822. https://doi.org/10.1016/j.watres.2011.04.038.

Krasner, S.W., Glaze, W.H., Weinberg, H.S., Daniel, P.A., Najm, I.N., 1993. Formation and control of bromate during ozonation of waters containing bromide. J. Am. Water Works Assoc. 85 (1), 73–81. https://doi.org/10.1002/j.1551-8833.1993.tb05923.x.

Kumar, N.M., Sudha, M.C., Damodharam, T., Varjani, S., 2020. Micro-pollutants in surface water: impacts on the aquatic environment and treatment technologies. In: Current Developments in Biotechnology and Bioengineering. Elsevier, pp. 41–62.

Lee, Y., Gerrity, D., Lee, M., Bogeat, A.E., Salhi, E., Gamage, S., Trenholm, R.A., Wert, E.C., Snyder, S.A., von Gunten, U., 2013. Prediction of micropollutant elimination during ozonation of municipal wastewater effluents: use of kinetic and water specific information. Environ. Sci. Technol. 47 (11), 5872–5881. https://doi.org/10.1021/es400781r.

Lehmkuhl, S., Wiese, M., Schubert, L., Held, M., Küppers, M., Wessling, M., Blümich, B., 2018. Continuous hyperpolarization with parahydrogen in a membrane reactor. J. Magn. Res. 291, 8–13. https://doi.org/10.1016/j.jmr.2018.03.012

.

Luo, Y., Guo, W., Ngo, H.H., Nghiem, L.D., Hai, F.I., Zhang, J., Liang, S., Wang, X.C., 2014. A review on the occurrence of micropollutants in the aquatic environment and their fate and removal during wastewater treatment. Sci. Total Environ. 473–474, 619–641. https://doi.org/10.1016/j.scitotenv.2013.12.065.

Mathon, B., Coquery, M., Liu, Z., Penru, Y., Guillon, A., Esperanza, M., Miège, C., Choubert, J.-M., 2021. Ozonation of 47 organic micropollutants in secondary treated municipal effluents: direct and indirect kinetic reaction rates and modelling. Chemosphere 262, 127969. https://doi.org/10.1016/j.chemosphere.2020.127969.

Merle, T., Pronk, W., von Gunten, U., 2017. Membro 3 x, a novel combination of a membrane contactor with advanced oxidation (o 3 /h 2 o 2) for simultaneous micropollutant abatement and bromate minimization. Environ. Sci. Technol. Lett. 4 (5), 180–185. https://doi.org/10.1021/acs.estlett.7b00061.

Nawrocki, J., Świetlik, J., Raczyk-Stanisławiak, U., Dabrowska, A., Biłozor, S., Ilecki, W., 2003. Influence of ozonation conditions on aldehyde and carboxylic acid formation. Ozone Sci. Eng. 25 (1), 53–62. https://doi.org/10.1080/713610650.

Pines, D.S., Min, K.-N., Ergas, S.J., Reckhow, D.A., 2005. Investigation of an ozone membrane contactor system. Ozone Sci. Eng. 27 (3), 209–217. https://doi.org/10.1080/01919510590945750.

Pinkernell, U., von Gunten, U., 2001. Bromate minimization during ozonation: mechanistic considerations. Environ. Sci. Technol. 35 (12), 2525–2531. https://doi.org/10.1021/es001502f.

Rakness, K.L., Hunter, G., Lew, J., Mundy, B., Wert, E.C., 2018. Design considerations for cost-effective ozone mass transfer in sidestream systems. Ozone Sci. Eng. 40 (3), 159–172. https://doi.org/10.1080/01919512.2018.1424532.

Sabelfeld, M., Geißen, S.-U., 2019. Effect of helical structure on ozone mass transfer in a hollow fiber membrane contactor. J. Membr. Sci. 574, 222–234. https://doi.org/10.1016/j.memsci.2018.10.056.

Sander, R., 2023. Compilation of Henry's law constants (version 5.0.0) for water as solvent. Atmos. Chem. Phys. 23 (19), 10901–12440. https://doi.org/10.5194/acp-23-10901-2023.

Schmitt, A., Mendret, J., Brosillon, S., 2022. Evaluation of an ozone diffusion process using a hollow fiber membrane contactor. Chem. Eng. Res. Des. 177, 291–303. https://doi.org/10.1016/j.cherd.2021.11.002.

Schmitt, A., Chevarin, C., Mendret, J., Brosillon, S., Bouyer, D., 2023. 3-d computational fluid dynamics modeling of a hollow fiber membrane contactor ozonation process. J. Water Proc. Eng. 51, 103362. https://doi.org/10.1016/j.jwpe.2022.103362.

Schollée, J.E., Bourgin, M., von Gunten, U., McArdell, C.S., Hollender, J., 2018. Non-target screening to trace ozonation transformation products in a wastewater treatment train including different post-treatments. Water Res. 142, 267–278. https://doi.org/10.1016/j.watres.2018.05.045.

Shin, J., Hidayat, Z.R., Lee, Y., 2016. Influence of seasonal variation of water temperature and dissolved organic matter on ozone and oh radical reaction kinetics during ozonation of a lake water. Ozone Sci. Eng. 38 (2), 100–114. https://doi.org/10.1080/01919512.2015.1079120.

Smith, D.W., El-Din, M.G., 2002. Theoretical analysis and experimental verification of ozone mass transfer in bubble columns. Environ. Technol. 23 (2), 135–147. https://doi.org/10.1080/09593332508618420.

Sohn, J., Amy, G., Cho, J., Lee, Y., Yoon, Y., 2004. Disinfectant decay and disinfection by-products formation model development: chlorination and ozonation by-products. Water Res. 38 (10), 2461–2478. https://doi.org/10.1016/j.watres.2004.03.009.

Soltermann, F., Abegglen, C., Götz, C., von Gunten, U., 2016. Bromide sources and loads in Swiss surface waters and their relevance for bromate formation during wastewater ozonation. Environ. Sci. Technol. 50 (18), 9825–9834. https://doi.org/10.1021/acs.est.6b01142.

Soltermann, F., Abegglen, C., Tschui, M., Stahel, S., von Gunten, U., 2017. Options and limitations for bromate control during ozonation of wastewater. Water Res. 116, 76–85. https://doi.org/10.1016/j.watres.2017.02.026.

Song, R., Donohoe, C., Minear, R., Westerhoff, P., Ozekin, K., Amy, G., 1996. Empirical modeling of bromate formation during ozonation of bromide-containing waters. Water Res. 30 (5), 1161–1168. https://doi.org/10.1016/0043-1354(95)00302-9.

Staehelin, J., Hoigne, J., 1982. Decomposition of ozone in water: rate of initiation by hydroxide ions and hydrogen peroxide. Environ. Sci. Technol. 16 (10), 676–681. https://doi.org/10.1021/es00104a009.

Staehelin, J., Buehler, R.E., Hoigne, J., 1984. Ozone decomposition in water studied by pulse radiolysis. 2. Hydroxyl and hydrogen tetroxide (ho4) as chain intermediates. J. Phys. Chem. 88 (24), 5999–6004. https://doi.org/10.1021/j150668a051.

Stylianou, S.K., Katsoyiannis, I.A., Mitrakas, M., Zouboulis, A.I., 2018. Application of a ceramic membrane contacting process for ozone and peroxone treatment of micropollutant contaminated surface water. J. Hazard. Mater. 358, 129–135. https://doi.org/10.1016/j.jhazmat.2018.06.060.

Tay, K.S., Rahman, N.A., Abas, M.R.B., 2013. Ozonation of metoprolol in aqueous solution: ozonation by-products and mechanisms of degradation. Environ. Sci. Pollut. Res. Int. 20 (5), 3115–3121. https://doi.org/10.1007/s11356-012-1223-3.

Tepper, M., Eminoglu, Y., Mehling, N., Walorski, J., Roth, H., Wessling, M., 2022b. Rotation-in-a-spinneret integrates static mixers inside hollow fiber membranes. J. Membr. Sci. 656, 120599. https://doi.org/10.1016/j.memsci.2022.120599.

Tepper, M., Fehlemann, L., Rubner, J., Luelf, T., Roth, H., Wessling, M., 2022a. Rotating microstructured spinnerets produce helical ridge membranes to overcome mass transfer limitations. J. Membr. Sci. 643, 119988. https://doi.org/10.1016/j.memsci.2021.119988.

Tepper, M., Padligur, M., Wypysek, D., Budeus, L., Mueller-Dott, J., Roth, H., Wessling, M., 2023. Helical-ridge-membranes from pvdf for enhanced gas–liquid mass transfer. J. Membr. Sci. 673, 121471. https://doi.org/10.1016/j.memsci.2023.121471.

Tomiyasu, H., Fukutomi, H., Gordon, G., 1985. Kinetics and mechanism of ozone decomposition in basic aqueous solution. Inorg. Chem. 24 (19), 2962–2966. https://doi.org/10.1021/ic00213a018.

von Gunten, U., 2003. Ozonation of drinking water: part I. Oxidation kinetics and product formation. Water Res. 37 (7), 1443–1467. https://doi.org/10.1016/S0043-1354(02)00457-8.

von Sonntag, C., 2007. The basics of oxidants in water treatment. Part a: Oh radical reactions. Water Sci. Technol., J. Int. Assoc. Water Pollut. Res. 55 (12), 19–23. https://doi.org/10.2166/wst.2007.383.

von Sonntag, C., von Gunten, U., 2012. Chemistry of Ozone in Water and Wastewater Treatment: From Basic Principles to Applications. IWA Publishing.

Wardenier, N., Liu, Z., Nikiforov, A., van Hulle, S.W.H., Leys, C., 2019. Micropollutant elimination by o3, uv and plasma-based aops: an evaluation of treatment and energy costs. Chemosphere 234, 715–724. https://doi.org/10.1016/j.chemosphere.2019.06.033.

Wenten, I.G., Julian, H., Panjaitan, N.T., 2012. Ozonation through ceramic membrane contactor for iodide oxidation during iodine recovery from brine water. Desalination 306, 29–34. https://doi.org/10.1016/j.desal.2012.08.032.

Westerhoff, P., Song, R., Amy, G., Minear, R., 1998. Numerical kinetic models for bromide oxidation to bromine and bromate. Water Res. 32 (5), 1687–1699. https://doi.org/10.1016/S0043-1354(97)00287-X.

Wünsch, R., Hettich, T., Prahtel, M., Thomann, M., Wintgens, T., von Gunten, U., 2022. Tradeoff between micropollutant abatement and bromate formation during ozonation of concentrates from nanofiltration and reverse osmosis processes. Water Res. 221, 118785. https://doi.org/10.1016/j.watres.2022.118785.

Xing, W., Yin, M., Lv, Q., Hu, Y., Liu, C., Zhang, J., 2014. Oxygen solubility, diffusion coefficient, and solution viscosity. In: Rotating Electrode Methods and Oxygen Reduction Electrocatalysts. Elsevier, pp. 1–31.

Yong, E.L., Lin, Y.-P., 2013. Kinetics of natural organic matter as the initiator, promoter, and inhibitor, and their influences on the removal of ibuprofen in ozonation. Ozone Sci. Eng. 35 (6), 472–481. https://doi.org/10.1080/01919512.2013.820641.

Zhou, H., Smith, D.W., Stanley, S.J., 1994. Modeling of dissolved ozone concentration profiles in bubble columns. J. Environ. Eng. 120 (4), 821–840. https://doi.org/10.1061/(ASCE)0733-9372(1994)120:4(821).

Zhou, H., Liu, J., Xia, H., Zhang, Q., Ying, T., Hu, T., 2015. Removal and reduction of selected organic micro-pollutants in effluent sewage by the ozone-based oxidation processes. Chem. Eng. J. 269, 245–254. https://doi.org/10.1016/j.cej.2015.01.116.